A light-induced charge order mode in a metastable cuprate ladder

Hari Padma,[1,2,*] Prakash Sharma,[3] Sophia F. R. TenHuisen,[1,4] Filippo Glerean,[1,†] Antoine Roll,[5] Pan Zhou,[3] Sarbajaya Kundu,[6,7] Arnau Romaguera,[8] Elizabeth Skoropata,[8] Hiroki Ueda,[8] Biaolong Liu,[8] Eugenio Paris,[8] Yu Wang,[9,10] Seng Huat Lee,[9,10] Zhiqiang Mao,[9,10] Mark P. M. Dean,[5] Edwin W. Huang,[6,7] Elia Razzoli,[8] Yao Wang,[3] and Matteo Mitrano[1,‡]

[1]*Department of Physics, Harvard University, Cambridge, MA, USA*

[2]*Department of Physics, Case Western Reserve University, Cleveland, OH, USA*

[3]*Department of Chemistry, Emory University, Atlanta, GA, USA*

[4]*Department of Applied Physics, Harvard University, Cambridge, MA, USA*

[5]*Condensed Matter Physics and Materials Science Department, Brookhaven National Laboratory, Upton, NY, USA*

[6]*Department of Physics and Astronomy, University of Notre Dame, Notre Dame, IN, USA*

[7]*Stavropoulos Center for Complex Quantum Matter, University of Notre Dame, Notre Dame, IN, USA*

[8]*PSI Center for Photon Science, Paul Scherrer Institute, Villigen, Switzerland*

[9]*Department of Physics, Pennsylvania State University, University Park, PA, USA*

[10]*2D Crystal Consortium, Materials Research Institute, Pennsylvania State University, University Park, PA, USA*

SUPPLEMENTAL MATERIAL

1. trXAS measurements

We present trXAS data with the x-ray polarizations (1.1) $E \parallel a$ and (1.2) $E \parallel c$, together with their respective fit functions. The pump pulses are polarized along the ladder legs ($E_{\text{pump}} \parallel c$) in all measurements.

1.1. $E \parallel a$

The O K-edge trXAS spectra ($E \parallel a$) feature two prominent peaks (see Fig. 1 of the main text, reproduced in Fig. S1). Prior work [1] demonstrated that the peak centered at 528 eV corresponds to the mobile carriers (Zhang-Rice singlets, ZRS), while the peak centered at 529.4 eV corresponds to the upper Hubbard band (UHB). Both peaks include overlapping contributions from the chain and ladder. The transfer of holes from chains to ladders by Ca substitution at equilibrium is empirically associated with a suppression of the ZRS and UHB, and an enhancement in between the peaks [1] (also see discussion in SI Section 4 of Ref. [2]).

We model the spectra as the sum of a Gaussian, a Lorentzian, and a linear function

$$I(\omega) = G(\omega; A_1, \omega_{01}, \sigma_1) + L(\omega; A_2, \omega_{02}, \sigma_2) + a\omega + b, \tag{1}$$

where the Gaussian $G(\omega; A_i, \omega_{0i}, \sigma_i)$ describes the Zhang-Rice singlet peak ($i = 1$), the Lorentzian $L(\omega; A_i, \omega_{0i}, \sigma_i)$ describes the upper Hubbard band ($i = 2$), and A, ω_0, and σ are the amplitude, center energy, and linewidth parameters. The fit parameters are shown in Table I.

Table I. Fit parameters for trXAS spectra ($E \parallel a$) in Fig. S1.

	A_1	ω_{01} (eV)	σ_1 (eV)	A_2	ω_{02} (eV)	σ_2 (eV)	a	b (eV)
Equilibrium	0.77(1)	527.96(1)	0.33(1)	0.55(2)	529.67(1)	0.43(1)	0.040(1)	-21(1)
$t = 0.4$ ps	0.80(1)	527.98(1)	0.36(1)	0.55(1)	529.66(1)	0.46(1)	0.039(1)	-21(1)
$t = 3$ ps	0.77(1)	527.98(1)	0.35(1)	0.48(3)	528.65(1)	0.42(1)	0.048(1)	-25(2)
$t = 101$ ps	0.79(1)	527.98(1)	0.35(3)	0.56(2)	529.67(4)	0.46(1)	0.038(1)	-20(1)

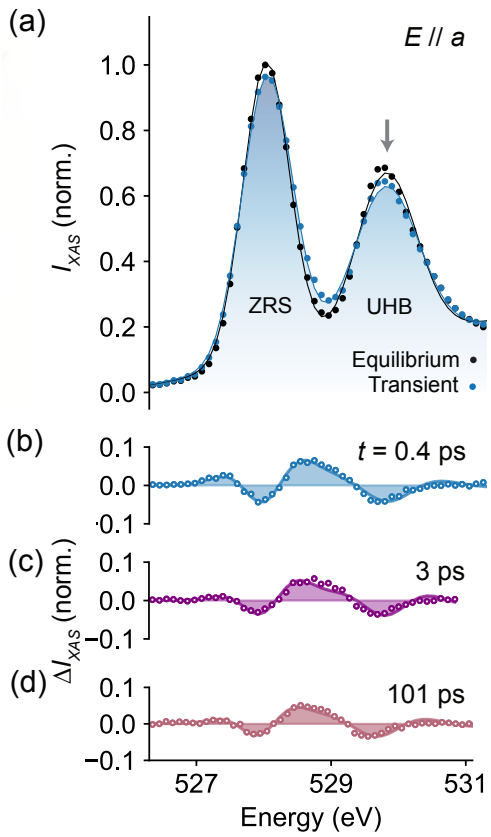

FIG. S1. (a) Equilibrium (black) and transient (blue, 6 mJ/cm^2 fluence) O K-edge trXAS at $t = 0.4$ ps. The x-ray pulses are polarized along the ladder rungs ($E \parallel a$), and the pump pulses are polarized along the ladder legs ($E \parallel c$), identical to the experimental conditions for the trRIXS measurements. (b-d) Differential trXAS intensity $[I_{\mathrm{XAS}}(t) - I_{\mathrm{XAS}}(t < 0)]$ at $t = 0.4$ ps, 3 ps, and 101 ps, respectively. The pump-induced spectral reshaping is metastable. The solid lines are fits to the data.

1.2. $E \parallel c$

The O K-edge trXAS spectra ($E \parallel c$) feature three peaks (see Fig. S2). Previous work [1] demonstrated that the peaks centered at 528 eV and 528.5 eV consist primarily of contributions from the chain and ladder Zhang-Rice singlets, respectively, while the peak centered at 529.4 eV includes overlapping contributions from the chain and ladder upper Hubbard bands. The transfer of holes from chains to ladders by Ca substitution at equilibrium is empirically associated with a suppression of the UHB, and an enhancement of the ZRS peaks [1, 2].

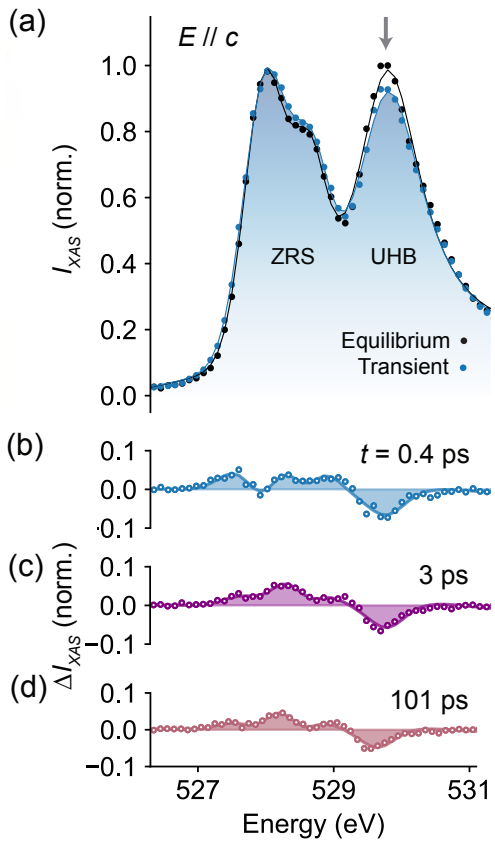

FIG. S2. (a) Equilibrium (black) and transient (blue, 6 mJ/cm^2 fluence) O K-edge trXAS at $t = 0.4$ ps. Pump and probe pulses are polarized along the ladder legs ($E \parallel c$). (b-d) Differential trXAS intensity $[I_{\mathrm{XAS}}(t) - I_{\mathrm{XAS}}(t < 0)]$ at $t = 0.4$ ps, 3 ps, and 101 ps, respectively. The pump-induced spectral reshaping is metastable. The solid lines are fits to the data.

We model the trXAS spectra as the sum of two Gaussians, a Lorentzian, and a linear function

$$I(\omega) = G(\omega; A_1, \omega_{01}, \sigma_1) + G(\omega; A_2, \omega_{02}, \sigma_2) + L(\omega; A_3, \omega_{03}, \sigma_3) + a\omega + b, \tag{2}$$

where the Gaussians $G(\omega; A_i, \omega_{0i}, \sigma_i)$ describe chain ($i = 1$) and ladder ($i = 2$) Zhang-Rice singlet peaks, and the Lorentzian $L(\omega; A_i, \omega_{0i}, \sigma_i)$ describes the upper Hubbard band ($i = 3$), and A, ω_0, and σ are the amplitude, center energy, and linewidth parameters. The fit parameters are shown in Table II.

Table II. Fit parameters for trXAS spectra ($E \parallel c$) in Fig. S2.

	A_1	ω_{01} (eV)	σ_1 (eV)	A_2	ω_{02} (eV)	σ_2 (eV)	A_3	ω_{03} (eV)	σ_3 (eV)	a	b (eV)
Equilibrium	0.60(3)	527.91(2)	0.28(1)	0.28(3)	528.54(2)	0.23(2)	1.63(6)	529.65(1)	0.58(2)	0.029(1)	-15(2)
$t = 0.4$ ps	0.66(3)	527.93(1)	0.32(1)	0.26(3)	528.57(2)	0.24(1)	1.64(6)	529.66(1)	0.63(2)	0.026(1)	-14(1)
$t = 3$ ps	0.63(3)	527.92(1)	0.29(1)	0.29(3)	528.53(2)	0.25(1)	1.68(5)	529.65(1)	0.63(2)	0.026(1)	-13(1)
$t = 101$ ps	0.60(3)	527.90(2)	0.29(1)	0.31(3)	528.53(2)	0.25(2)	1.62(6)	529.66(1)	0.62(2)	0.027(3)	-14(1)

2. trRIXS measurements

2.1. Equilibrium RIXS energy map

We plot a RIXS intensity map as a function of incident photon energy and energy loss in Fig. S3, together with the XAS spectrum. The Zhang-Rice singlet (ZRS) region is dominated by a substantial fluorescence signal. In contrast, at resonance with the upper Hubbard band (UHB) peak, there is no fluorescence in the spectral window of interest (< 1 eV), enabling a reliable interpretation of the trRIXS data acquired at this incident energy. Hence, all trRIXS measurements in this work are conducted with the incident photons resonant with the UHB.

2.2. Subtraction of dd excitations

We present the full set of trRIXS spectra in Fig. S4 and Fig. S5. All trRIXS spectra are normalized to the equilibrium integrated intensity of *dd* and charge transfer excitations from 1.3 eV to 10 eV.

˘The *dd* excitations of this material extend into the spectral region of interest and must be properly accounted for to isolate any new features that emerge upon optical excitation. To isolate spectral changes below 1 eV, we fit and subtract the *dd* excitations above 1.3 eV. We independently fit the equilibrium and transient trRIXS spectra between 1.3 eV and 2.8 eV to the sum of a skewed Gaussian and a Gaussian as shown in Fig. S6. The resulting spectra with the *dd* excitations' contribution removed are shown in Fig. S7. Energy-momentum colormaps of the *dd*-subtracted trRIXS data are presented in Fig. 3 of the main text. We additionally present identically formatted colormaps of the raw trRIXS data in Fig. S8.

Both the raw spectra and colormaps clearly display the same dispersive feature seen in the *dd*-subtracted colormaps, demonstrating that this spectral feature is robust and does not depend on the specific subtraction procedure. Hence, we use the *dd*-subtracted spectra as the basis for all subsequent analysis.

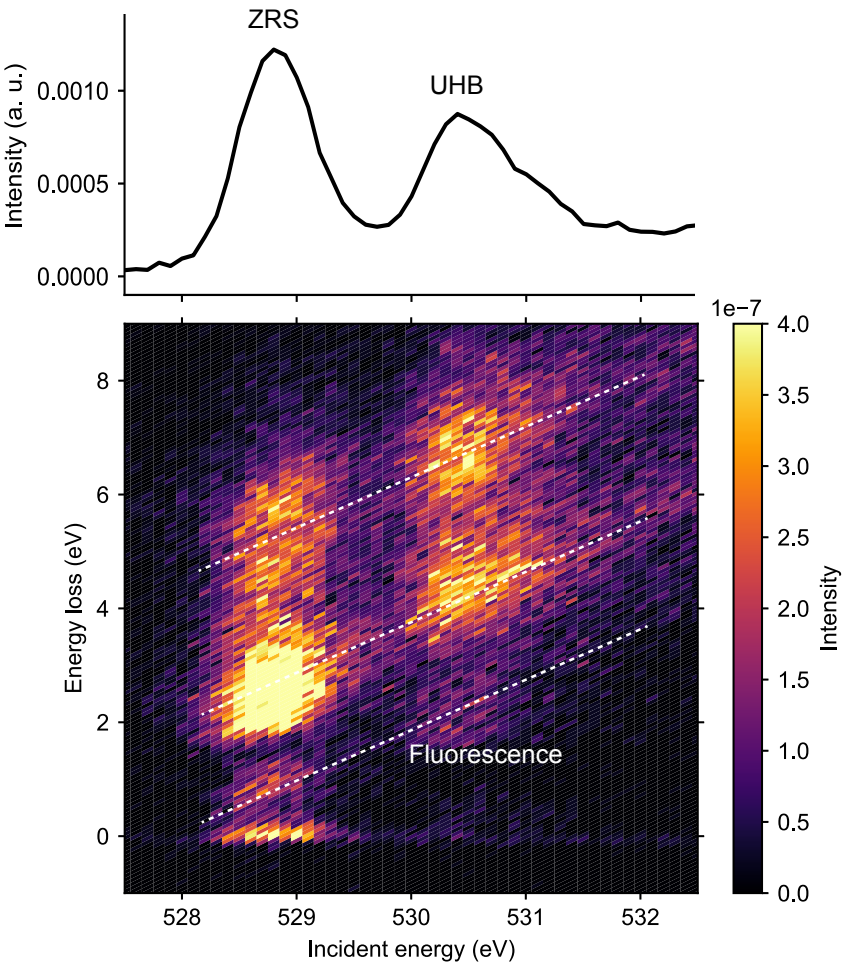

FIG. S3. RIXS intensity map plotted as a function of incident photon energy and energy loss, across the O K-edge. The white dashed line indicates fluorescence. (top) XAS spectrum obtained by integrating over energy loss.

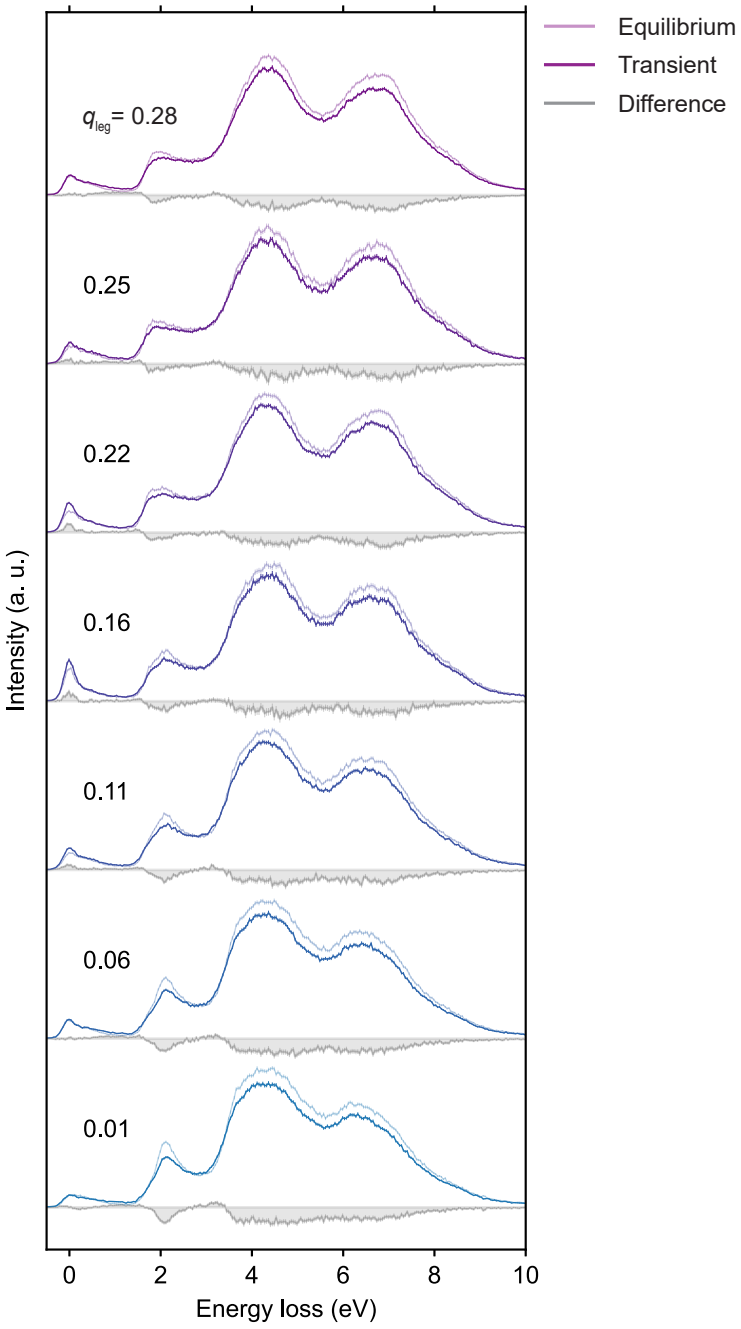

FIG. S4. Equilibrium, transient ($t = 0.4$ ps), and difference trRIXS spectra for momenta spanning $q_{\mathrm{leg}} = 0.01$ to 0.28 r.l.u. The spectra are vertically offset for clarity. All spectra are normalized to the equilibrium integrated intensity of *dd* and charge transfer excitations from 1.3 eV to 10 eV.

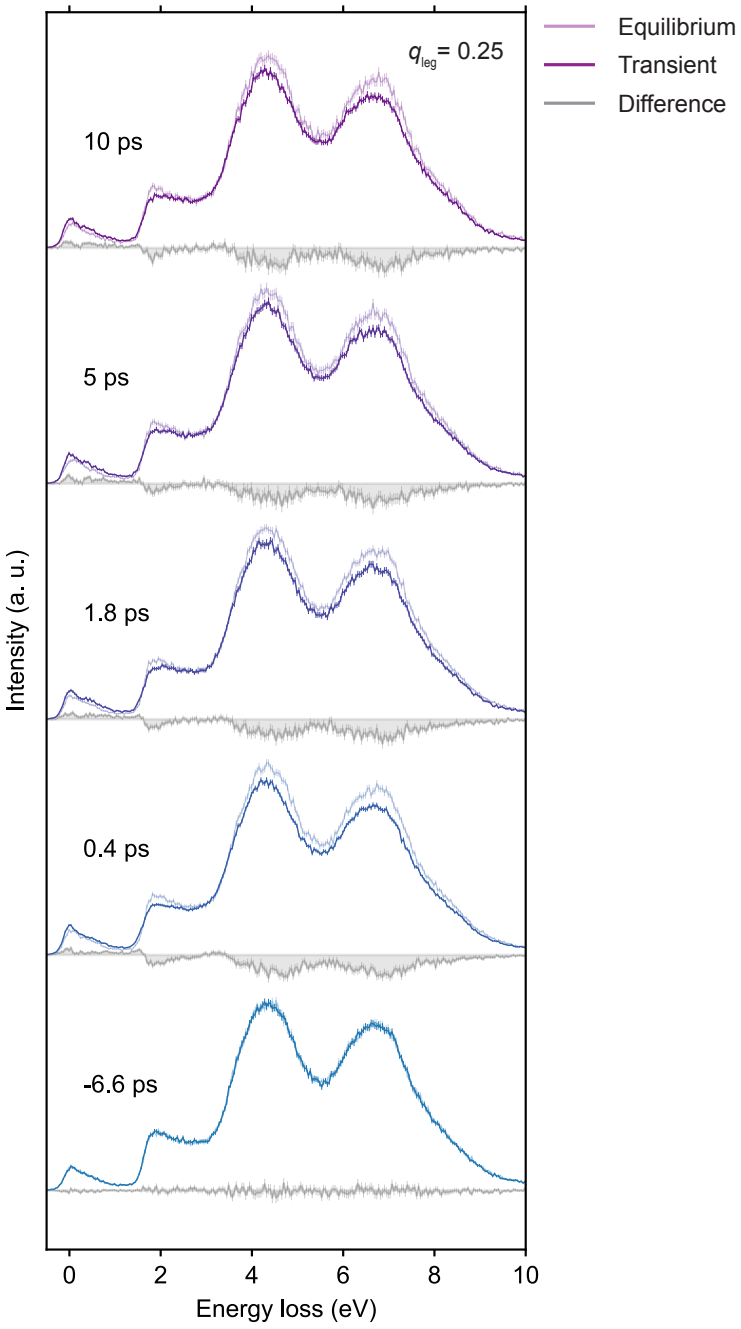

FIG. S5. Equilibrium, transient, and difference trRIXS spectra at $q_{\mathrm{leg}} = 0.25$ for delays spanning t = -6.6 to 10 ps. The spectra are vertically offset for clarity. All spectra are normalized to the equilibrium integrated intensity of *dd* and charge transfer excitations from 1.3 eV to 10 eV.

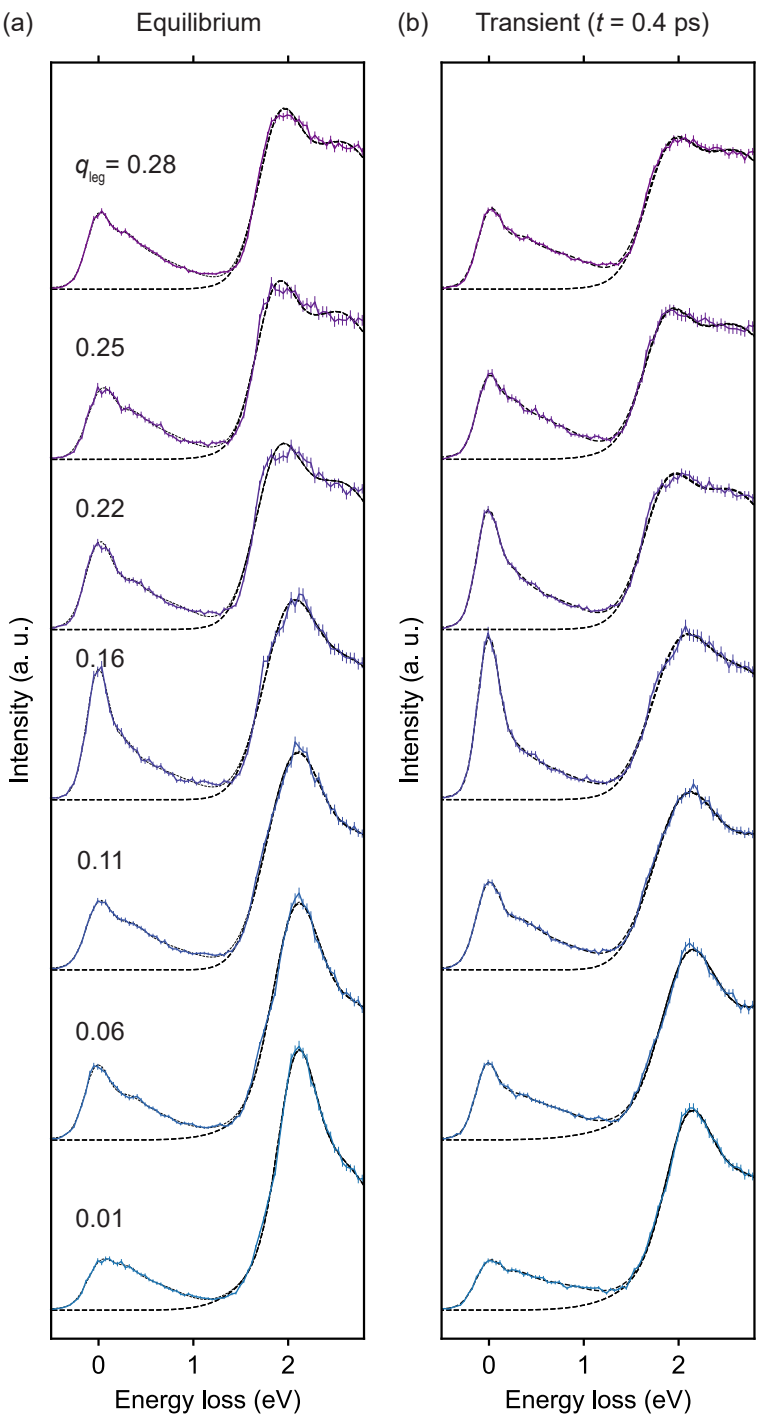

FIG. S6. (a) Equilibrium and (b) transient trRIXS spectra for momenta spanning $q_{\mathrm{leg}} = 0.01$ to 0.28 r.l.u. The dashed black lines are fits to the *dd* excitations between 1.3 eV and 2.8 eV. The spectra are vertically offset for clarity.

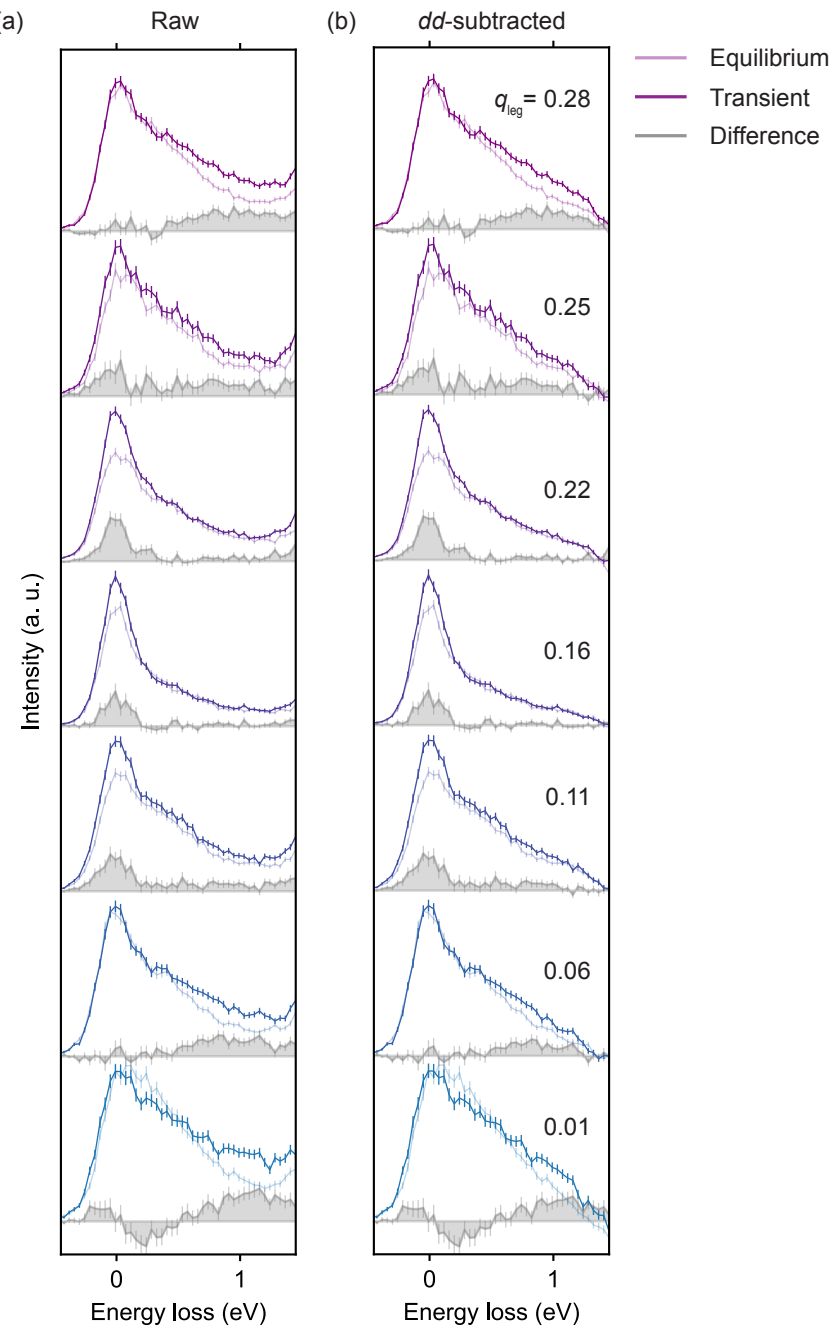

FIG. S7. Equilibrium, transient, and difference trRIXS spectra for momenta spanning $q_{\mathrm{leg}} = 0.01$ to 0.28 r.l.u. Panel (a) shows the raw spectra, and panel (b) shows the spectra with the *dd* excitations subtracted using the fits in Fig. S6. The spectra are vertically offset for clarity.

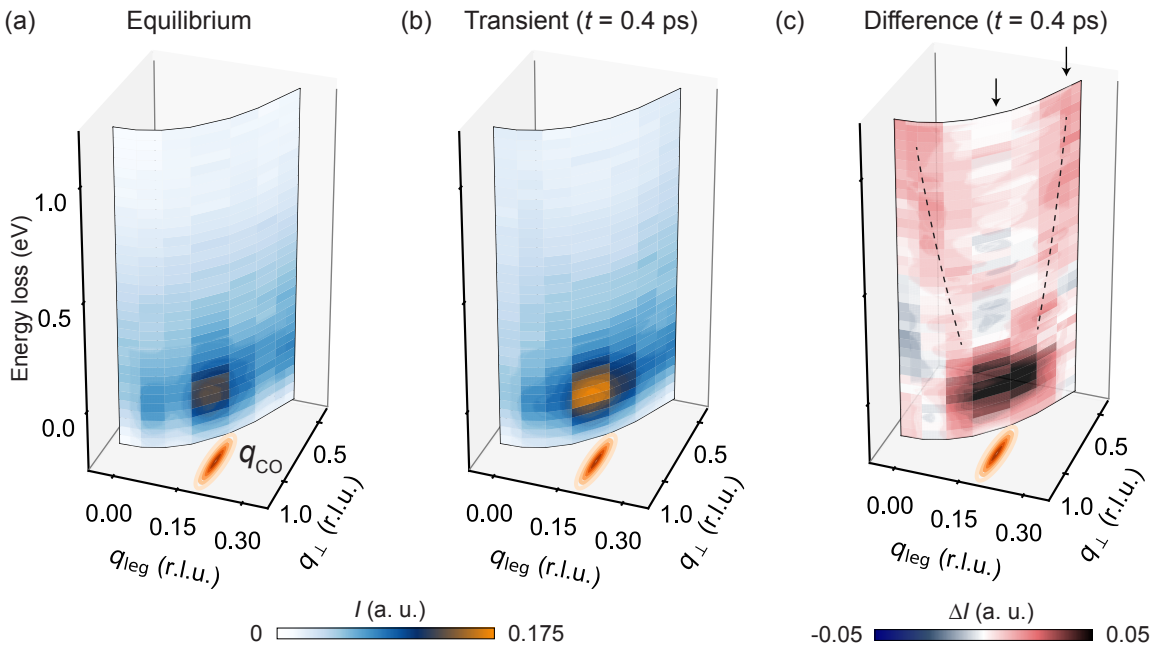

FIG. S8. Colormaps with the raw trRIXS data. (a-c) Equilibrium, transient, and difference trRIXS momentum-energy intensity maps using the raw data, as a function of q_{leg} and $q_{\perp}$, respectively. q_{CO} marks the charge order wavevector [3]. Dashed lines in (c) are guides to the eye.

2.3. Fitting trRIXS spectra

The O K-edge RIXS spectrum of $Sr_{14}Cu_{24}O_{41}$ is complex, and distinct from that at the Cu L-edge, with contributions from multiphonons, two-triplon, and multi-triplon continua extending to higher energies, as demonstrated in Ref. [4]. We constrain our fitting procedure based on prior equilibrium O K-edge RIXS measurements [4], Cu L-edge trRIXS measurements [2], and prior theoretical results [5]. By systematically considering and excluding different possibilities, we show that a dispersive charge order mode provides the simplest and most plausible interpretation of our observations, as outlined below.

First, since the pump-induced spectral changes extend up to ∼1 eV, multiphonon excitations, which are below ∼0.2 eV, can be excluded as their origin. Next, we consider the possibility of a reshaping of the multi-triplon continuum, in particular a momentum-dependent redistribution of spectral weight. As shown in theoretical work by Schmidt and Uhrig [5] (see Fig. 3 therein), the even-n channel of the $\Delta S = 0$ triplon continuum (detected in our O K-edge RIXS measurements) is almost entirely accounted for by two-triplon and four-triplon excitations. The lower-energy portion of the continuum is dominated by two-triplons, while the higher-energy portion arises from four-triplons. The enhancement in spectral weight at higher energies observed in our trRIXS spectra could therefore imply an increase of the four-triplon contribution at the expense of the two-triplons, for example through a suppression of the rung exchange or a renormalization of the effective ring exchange. However, Ref. [5] shows that such an enhancement of the $\Delta S = 0$ four-triplon contribution must be accompanied by an enhancement of the $\Delta S = 1$ two-triplon response. This expectation is incompatible with our prior Cu L-edge trRIXS measurements, which instead show an unambiguous suppression of the $\Delta S = 1$ two-triplon signal. This inconsistency rules out an interpretation in terms of a reshaping of the $\Delta S = 0$ multi-triplon continuum driven by renormalized exchange couplings in the metastable state. We further note that the momentum-dependent spectral weight enhancement observed in our data, without a corresponding suppression elsewhere in the spectrum, is inconsistent with a simple broadening of the multi-triplon continuum. Moreover, any model invoking a reshaped multi-triplon continuum would require fine tuning to reproduce the symmetric dispersion about q_{CO}, necessitating additional and ad hoc couplings between triplons and the charge order.

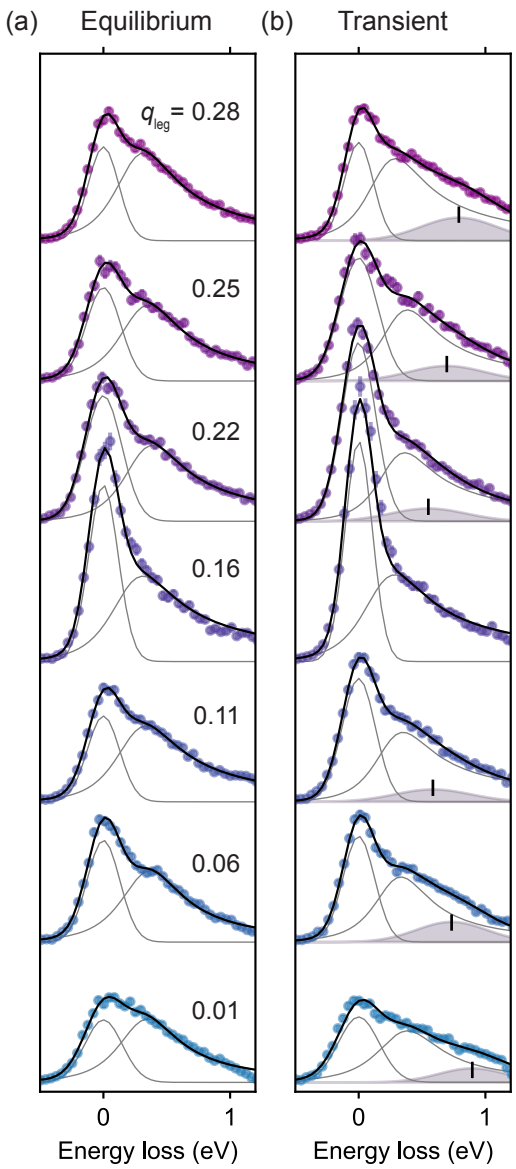

FIG. S9. (a) Equilibrium and (b) transient trRIXS spectra for momenta spanning $q_{\mathrm{leg}} = 0.01$ to 0.28 r.l.u., fit using the functional form described in the text. Black lines denote the total fits, thin grey lines the individual components. The transient spectra are fit with an additional Gaussian, denoted by grey shaded areas. The spectra are vertically offset for clarity.

Having excluded phonons and multi-triplon continua, the pump-induced spectral feature is most naturally interpreted as a new excitation. The equilibrium spectra are fit to the sum of a Gaussian and an asymmetric Lorentzian

$$I(\omega) = G(\omega; A_1, \omega_{01}, \sigma_1) + AL(\omega; A_2, \omega_{02}, \sigma_2, \gamma_2), \tag{3}$$

where the Gaussian $G(\omega; A_1, \omega_{01} = 0, \sigma_1)$ describes the elastic peak, and the asymmetric Lorentzian $AL(\omega; A_2, \omega_{02}, \sigma_2, \gamma_2)$ (commonly used to fit multimagnon continua, see [6–8]) describes the triplon continuum [Fig. S9(a)], and A, ω_{0i}, σ_i, and γ_i are the amplitude, center energy, linewidth, and asymmetry parameters.

We constrain the equilibrium two-triplon parameters to ensure a non-dispersive peak center, consistent with prior high-resolution RIXS measurements [4]. In the transient spectra, we include an additional Gaussian $G(\omega; A_3, \omega_{03}, \sigma_3)$ to capture the high-energy enhancement. In the transient fits, the two-triplon frequency, linewidth, and asymmetry are constrained to vary by less than 20% relative to their equilibrium values, and the two-triplon amplitude is restricted to not exceed its equilibrium value. The resulting best-fit parameters are reported in Table III and Table IV. We plot the full set of fits in Fig. S9.

Table III. Fit parameters for equilibrium trRIXS spectra in Fig. S9.

q_{leg} (r.l.u.)	A_1	σ_1 (eV)	A_2	ω_{02} (eV)	σ_2 (eV)	γ_2
0.01	0.25	0.15	0.71	0.41	0.34	-2.1
0.06	0.35	0.13	0.80	0.42	0.34	-2.0
0.11	0.29	0.13	1.07	0.45	0.46	-2.8
0.16	0.55	0.12	1.46	0.48	0.59	-3.0
0.22	0.48	0.14	1.03	0.50	0.45	-3.0
0.25	0.34	0.14	0.94	0.44	0.39	-2.5
0.28	0.30	0.12	1.15	0.42	0.42	-2.9
Std. Err.*	0.02	0.01	0.05	0.02	0.02	0.5

*The maximum standard error for each set of momentum-dependent parameters is listed in the last row.

In assigning the new dispersive feature, we considered all plausible possibilities, taking into account the observed propagation velocity, dispersion, and energy scale, as outlined in the main text. Within these constraints, a charge excitation provides the most consistent explanation. In contrast to scenarios based on reshaped triplon continua, the symmetric dispersion about q_{CO} is naturally explained in terms of charge order fluctuations.

Finally, $Sr_{14}Cu_{24}O_{41}$ also hosts a distinct superlattice peak associated with charge order in the chains [9]. However, the ladder charge order peak is centered near $q_{\text{CO}} \simeq (0, 0, 0.20)$ r.l.u.

Table IV. Fit parameters for transient trRIXS spectra in Fig. S9.

q_{leg} (r.l.u.)	A_1	σ_1 (eV)	A_2	ω_{02} (eV)	σ_2 (eV)	γ_2	A_3	ω_{03} (eV)	σ_3 (eV)
0.01	0.28	0.16	0.58	0.43	0.34	-1.8	0.10	0.90	0.27
0.06	0.35	0.12	0.67	0.39	0.31	-2.4	0.15	0.73	0.28
0.11	0.44	0.13	1.02	0.49	0.50	-3.4	0.10	0.59	0.30
0.16	0.63	0.11	1.53	0.46	0.62	-3.1	0.00	-	-
0.22	0.63	0.13	0.95	0.49	0.47	-3.5	0.10	0.55	0.30
0.25	0.49	0.15	0.82	0.47	0.37	-3.0	0.12	0.69	0.30
0.28	0.30	0.11	1.06	0.39	0.42	-3.1	0.19	0.80	0.30
Std. Err.*	0.05	0.01	0.40	0.08	0.20	0.7	0.05	0.10	0.05

*The maximum standard error for each set of momentum-dependent parameters is listed in the last row.

whereas the chain superlattice peak is located at $q \simeq (0, 0, 0.45)$ r.l.u. (both values specified in ladder units, $c_{\mathrm{L}} = 3.95$ Å). This separation in momentum space is sufficiently large that the chain peak does not overlap with, and is not expected to contribute appreciably to, the momentum range accessed in our trRIXS measurements. We therefore attribute the observed transient dispersive mode predominantly to charge order fluctuations in the ladders.

3. RPA calculations

To check whether plasmons in a system with a charge density wave (CDW) can give rise to modes near q_{CDW}, we perform a calculation using the random phase approximation (RPA) for a two-leg ladder system. Under the RPA, the loss function is given by

$$L(\mathbf{q},\omega) = -\mathrm{Im}\frac{1}{1 - V(\mathbf{q})\chi_0(\mathbf{q},\omega)}. \tag{4}$$

We use the interaction for a layered electron gas [10, 11]

$$V(\mathbf{q}) = \frac{V_0}{q_\parallel}\frac{\sinh(q_\parallel c)}{\cosh(q_\parallel c) - \cos(q_z c)}, \tag{5}$$

where $q_\parallel$ is in-plane momentum transfer, and χ_0 the Lindhard function

$$\chi_0(\mathbf{q},\omega) = \frac{1}{N}\sum_{\mathbf{k}}\frac{f_{\mathbf{k}} - f_{\mathbf{k}+\mathbf{q}}}{\omega + i0^+ + \epsilon_{\mathbf{k}} - \epsilon_{\mathbf{k}+\mathbf{q}}} \tag{6}$$

where $N = 2500$ is the number of k-points; $f_{\mathbf{k}} = [e^{(\epsilon_{\mathbf{k}}-\mu)/T} + 1]^{-1}$ at temperature T, which we set to 0; and $\epsilon_{\mathbf{k}}$ is the non-interacting dispersion. We tune the interaction strength V_0 to get a plasmon around 0.5 eV at $q = 0$. The results are qualitatively identical for any reasonable choice of V_0. As can be seen in the left panels of Fig. S10, tuning q_z can turn the plasmon acoustic at small in-plane $q_\parallel$.

We treat the effects of a CDW at mean-field level by adding to our Hamiltonian a potential

$$H_\Delta = \Delta\sum_i \cos\left(\frac{2\pi}{\lambda}x_i\right)\hat{n}_i, \tag{7}$$

where $\lambda = 5a$ is the CDW period. The loss function for $\Delta = 0.2$ eV is shown in the right panels of Fig. S10. The main effect of the CDW is to break up the plasmon dispersion, due to the more complicated structure of the multi-band Lindhard function resulting in additional Landau damping in some regions. There is no collective mode or "folding" associated with the plasmon, and no special behavior near $q_{\mathrm{CDW}} = 0.2$ r.l.u.

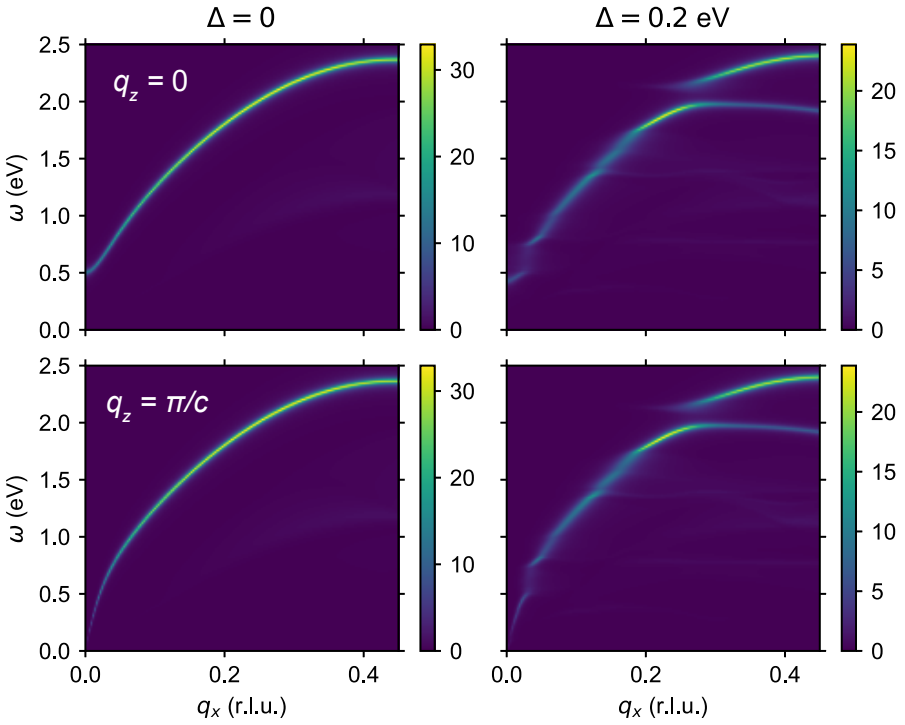

FIG. S10. Random phase approximation (RPA) calculations of the loss function, showing expected plasmon behaviors, with or without a CDW order parameter Δ, and at $q_z = 0$ or $q_z = \pi/c$.

4. DMRG calculations

The minimal model for the ladder subunits of $Sr_{14}Cu_{24}O_{41}$ is the two-leg extended Hubbard model [8], described by the Hamiltonian:

$$\begin{aligned}\hat{H} = &-t\sum_{i,\lambda,\sigma}\left(c^{\dagger}_{i,\lambda\sigma}c_{i+1,\lambda\sigma} + \text{h.c.}\right) - t_{\perp}\sum_{i,\sigma}\left(c^{\dagger}_{i,1\sigma}c_{i,2\sigma} + \text{h.c.}\right) \\ &- t'\sum_{i,\sigma}\left(c^{\dagger}_{i,1\sigma}c_{i+1,2\sigma} + \text{h.c.}\right) + U\sum_{i,\lambda} n_{i,\lambda\uparrow}n_{i,\lambda\downarrow} + V\sum_{i,\lambda} n_{i\lambda}\hat{n}_{i+1,\lambda}\end{aligned} \tag{8}$$

where $c^{\dagger}_{i,\lambda\sigma}$ ($c_{i,\lambda\sigma}$) creates (annihilates) an electron on rung i with chain index $\lambda \in \{1,2\}$ and spin $\sigma \in \{\uparrow,\downarrow\}$, $n_{i,\lambda} = \sum_{\sigma} n_{i,\lambda\sigma}$ is the electron number operator, t and $t_{\perp}$ are the nearest-neighbor hopping strengths along chain and rung directions, respectively, t' is the next-nearest-neighbor (diagonal) hopping between the chains, and U is the onsite Coulomb interaction. Recent studies have revealed that the nearest-neighbor attractive $V \sim -t$ is necessary to accurately model one-dimensional cuprates [8, 12, 13].

We adopt the model parameters from previous fits to experimental data [8], with $U = 8t$, $t_{\perp} = 0.84t$, and $t' = -0.3t$, where $t \simeq 0.38$ eV for cuprate ladders. Large attractive interactions ($-V > t$) can complicate the computation of long-range correlations due to the proximity to phase separation, hence we fix $V = -0.8t$ in our calculations. We note that our final results are not strongly dependent on the value of V. To ensure DMRG convergence, we perform 31 sweeps and keep the largest singular eigenvalues up to 5600, which yields a truncation error below $\epsilon = 10^{-6}$ for a ladder of length $L = 100$ with open boundary conditions.

To analyze the charge properties in the cuprate ladder ground state, we calculate the real-space distribution of charge correlation $D(r) = \langle n_i n_{i+r}\rangle - \langle n_i\rangle\langle n_{i+r}\rangle$. Due to the sensitivity of the correlation exponents to the choice of the reference bond, we obtain more accurate estimates by averaging over a string of different reference sites in the bulk. We plot $D(r)$ on a logarithmic scale for selected hole densities p in Fig. S11(a). The charge correlations exhibit a power-law decay at long distances, $D(r) \propto r^{-K_{\alpha}}$, characterized by the charge exponent K_{ρ}. We plot the extracted exponents as a function of hole density p in Fig. S11(b).

The charge correlations exhibit a clear crossover in behavior with increasing doping. At low doping levels, our calculations reveal a charge density wave ground state [see Fig. S11(a)], with highly suppressed long-range charge fluctuations, as indicated by the large

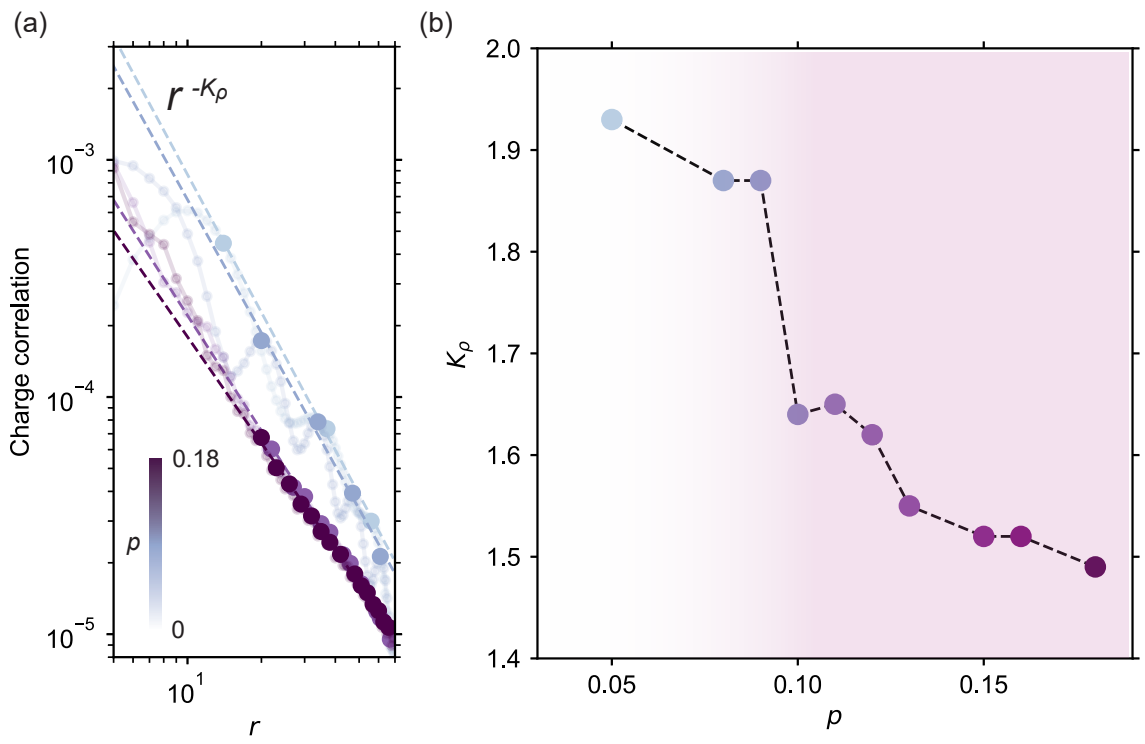

FIG. S11. Ground-state DMRG results for two-leg extended Hubbard ladder. (a) The real-space distribution of the charge correlation $D(r)$ at a few representative hole densities p, plotted on a logarithmic scale along both axes. The dashed lines are power law fits, $D(r) \propto r^{-K_\alpha}$. (b) The extracted power law exponents K_ρ as a function of hole density.

exponents K_ρ. At larger doping, K_ρ sharply drops at $p \sim 0.1$ [see Fig. S11(b)], together with a quenching of the charge density wave. This sharp drop in K_ρ signifies a rapid increase in the charge susceptibility, supporting the emergence of enhanced charge fluctuations seen experimentally.

* hari.padma@case.edu

† Present address: Condensed Matter Physics and Materials Science Department, Brookhaven National Laboratory, Upton, NY, USA

‡ mmitrano@g.harvard.edu

[1] N. Nücker, M. Merz, C. A. Kuntscher, S. Gerhold, S. Schuppler, R. Neudert, M. Golden, J. Fink, D. Schild, S. Stadler, *et al.*, Hole distribution in $(Sr,Ca,Y,La)_{14}Cu_{24}O_{41}$ ladder compounds studied by x-ray absorption spectroscopy, Physical Review B **62**, 14384 (2000).

[2] H. Padma, F. Glerean, S. F. R. TenHuisen, Z. Shen, H. Wang, L. Xu, J. D. Elliott, C. C. Homes, E. Skoropata, H. Ueda, B. Liu, E. Paris, A. Romaguera, B. Lee, W. He, Y. Wang, S. H. Lee, H. Choi, S.-Y. Park, Z. Mao, M. Calandra, H. Jang, E. Razzoli, M. P. M. Dean, Y. Wang, and M. Mitrano, Symmetry-protected electronic metastability in an optically driven cuprate ladder, Nature Materials **24**, 1584 (2025).

[3] P. Abbamonte, G. Blumberg, A. Rusydi, A. Gozar, P. Evans, T. Siegrist, L. Venema, H. Eisaki, E. Isaacs, and G. Sawatzky, Crystallization of charge holes in the spin ladder of $Sr_{14}Cu_{24}O_{41}$, Nature **431**, 1078 (2004).

[4] Y. Tseng, E. Paris, K. P. Schmidt, W. Zhang, T. C. Asmara, R. Bag, V. N. Strocov, S. Singh, J. Schlappa, H. M. Rønnow, *et al.*, Momentum-resolved spin-conserving two-triplon bound state and continuum in a cuprate ladder, Communications Physics **6**, 138 (2023).

[5] K. P. Schmidt and G. S. Uhrig, Spectral properties of magnetic excitations in cuprate two-leg ladder systems, Modern Physics Letters B **19**, 1179 (2005).

[6] J. Bertinshaw, J. K. Kim, J. Porras, K. Ueda, N.-H. Sung, A. Efimenko, A. Bombardi, J. Kim, B. Keimer, and B. J. Kim, Spin-wave gap collapse in Rh-doped Sr_2IrO_4, Physical Review B **101**, 094428 (2020).

[7] L. Martinelli, D. Betto, K. Kummer, R. Arpaia, L. Braicovich, D. Di Castro, N. B. Brookes, M. Moretti Sala, and G. Ghiringhelli, Fractional spin excitations in the infinite-layer cuprate $CaCuO_2$, Physical Review X **12**, 021041 (2022).

[8] H. Padma, J. Thomas, S. F. R. TenHuisen, W. He, Z. Guan, J. Li, B. Lee, Y. Wang, S. H. Lee, Z. Mao, H. Jang, V. Bisogni, J. Pelliciari, M. P. M. Dean, S. Johnston, and M. Mitrano, Beyond-Hubbard Pairing in a Cuprate Ladder, Phys. Rev. X **15**, 021049 (2025).

[9] A. Rusydi, P. Abbamonte, H. Eisaki, Y. Fujimaki, S. Smadici, N. Motoyama, S. Uchida, Y.-J. Kim, M. Rübhausen, and G. Sawatzky, Strain Amplification of the $4k_F$ Chain Instability in $Sr_{14}Cu_{24}O_{41}$, Physical Review Letters **100**, 036403 (2008).

[10] A. L. Fetter, Electrodynamics of a layered electron gas. II. Periodic array, Annals of Physics **88**, 1 (1974).

[11] M. Hepting, L. Chaix, E. Huang, R. Fumagalli, Y. Peng, B. Moritz, K. Kummer, N. Brookes, W. Lee, M. Hashimoto, *et al.*, Three-dimensional collective charge excitations in electron-doped copper oxide superconductors, Nature **563**, 374 (2018).

[12] Z. Chen, Y. Wang, S. N. Rebec, T. Jia, M. Hashimoto, D. Lu, B. Moritz, R. G. Moore, T. P.

Devereaux, and Z.-X. Shen, Anomalously strong near-neighbor attraction in doped 1D cuprate chains, Science **373**, 1235 (2021).

[13] Y. Wang, Z. Chen, T. Shi, B. Moritz, Z.-X. Shen, and T. P. Devereaux, Phonon-mediated long-range attractive interaction in one-dimensional cuprates, Physical Review Letters **127**, 197003 (2021).